ASEN 2502 Technical Note: Analysis of a Clark Y-14 Airfoil in a Low Speed Wind Tunnel

Cameron Lovejoy, Jamie Buckjune, Nicole Miltonberger, Sarvesh Chandrakumar, Lily Schimschal, and Robert Sullenger *

Nomenclature

A	=	amplitude of oscillation
a	=	cylinder diameter
C_p	=	pressure coefficient
Cx	=	force coefficient in the x direction
Cy	=	force coefficient in the y direction
c	=	chord
dt	=	time step
Fx	=	X component of the resultant pressure force acting on the vehicle
Fy	=	Y component of the resultant pressure force acting on the vehicle
f, g	=	generic functions
h	=	height
i	=	time index during navigation
j	=	waypoint index
K	=	trailing-edge (TE) nondimensional angular deflection rate
Θ	=	boundary-layer momentum thickness
ρ	=	density

Subscripts

cg	=	center of gravity
G	=	generator body
iso	=	waypoint index

*Undergraduate Student, Smead Aerospace Engineering Sciences, University of Colorado Boulder, 3775 Discovery Drive, Boulder, CO

I. Introduction

The objective of this experiment was to evaluate the performance of a Clark Y-14 airfoil to prepare for a future small-scale glider project and to compare the findings with the published NACA results from 1938[1]. The experiment consisted of testing the angles of attack from -14° to 15° in 1 degree increments at 15m/s and 30m/s. The airfoil spanned the entire width tunnel to simulate an infinite surface and included 16 pressure ports that collect surface pressure and store that data throughout 20 timesteps. This data is then used to compute the lift produced from this pressure distribution over the top and bottom surfaces of the airfoil. These computations allow for an understanding of how different aerodynamic forces act on the airfoil, and dictate future modifications based on this data. Overall, the main goal was to better understand the relationships between these aerodynamic principles and evaluate them at different angles of attack using a common airfoil shape.

II. Summary of Results

The velocity and pressure distributions change with angles of attack and match the expected aerodynamic behavior. At 0° angle of attack, the top and bottom surface distributions are not symmetric. With the upper surface having lower velocities and a lower pressure than the lower surface in the mid to aft chord region, notably near x/c 0.75. This makes sense for the Clark Y-14 airfoil since its cambered features cause it to generate lift even when set to zero degrees. At 6° angle of attack, the upper surface velocity increases near the leading edge, while the lower surface velocity decreases. Shown in the pressure distribution of Figure 1, the suction peak on the upper surface becomes more negative and the lower surface pressure increases, causing greater lift.

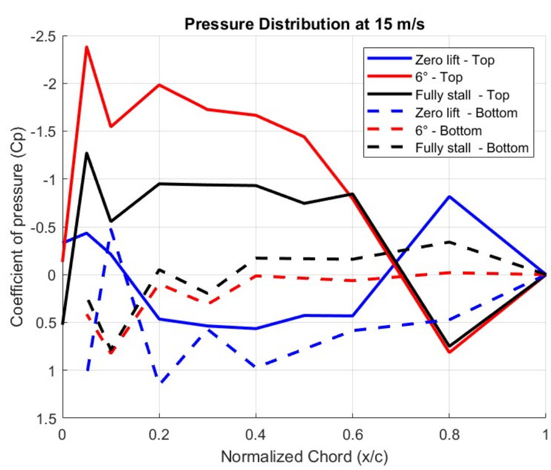

Fig. 1

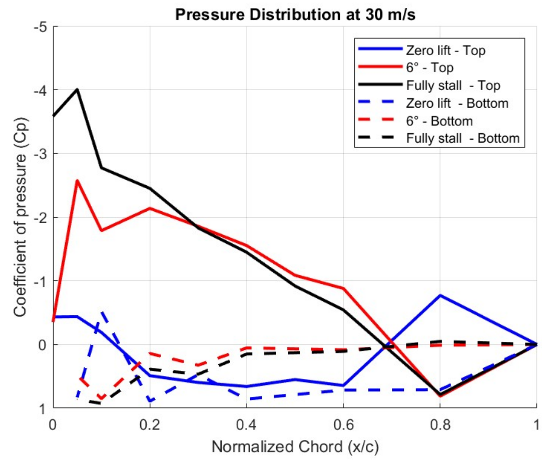

Fig. 2

The velocity (Figures 3 4) and pressure distributions (Figures 1 2) change with angles of attack and match the expected aerodynamic behavior which can be expressed with . In the velocity plots of Figure 3 and Figure 4, regions of higher flow speed correspond to lower static pressure, while slower flow corresponds to higher static pressure. For example, near the leading edge at 6° angle of attack, the upper surface velocity reaches values at around 55 m/s (Figure 3) which aligns with a suction peak in the pressure coefficient of nearly -2.5 (Figure 2). At the same time, the lower surface velocity falls to around 12 m/s, corresponding to a pressure coefficient of around 0.75. The resulting pressure difference across the airfoil surfaces produces a net upward force. This direct relationship between velocity and pressure distributions supports the theory that lift comes from the redistribution of velocity around the airfoil, with faster flow on the upper surface creating suction, and the slower flow on the lower surface increasing pressure.

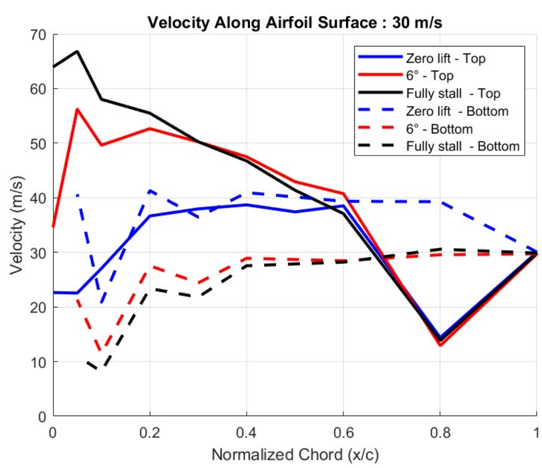

Fig. 3

The majority of lift is generated on the forward portion of the upper surface, near the leading edge. The velocity distribution of Figure 3 shows that at 6° angle of attack for 30m/s, the flow over the top surface increases to around 55 m/s within the first 20% of the chord, while the lower surface velocity remains lower around 10 - 25 m/s.

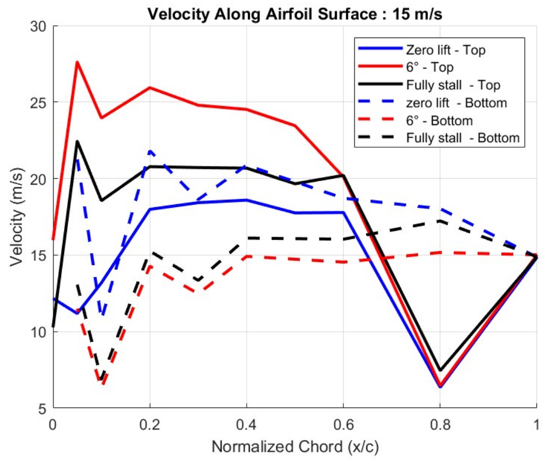

Fig. 4

Similarly, Figure 4 displays how for 6° angle of attack for 15 m/s, the flow on the top surface is around 20 to 25 m/s within the first 20% of the chord, while the lower surface velocity remains lower around 10 to 15 m/s. This acceleration for both speeds corresponds to a strong suction peak in the pressure distribution, where the pressure coefficient (Figure 1, 2) for both speeds on the upper surface goes to around -2.5, while the lower surface goes to around 0.3 - 0.6 in the leading edge. Since lift is the difference in pressure between the upper and lower surfaces, the large velocity increase and resulting suction peak in the forward 20% of the chord contributes to most of the lift. Around the middle to end of the chord, the velocity and pressure differences are smaller, so their contribution to lift is less significant.

After the leading edge suction peak on the upper surface, where the C_p for "Fully stall - Top" is -4 at x/c 0.5 for 30m/s (Figure 2). The C_p increases rapidly to about 0.7 near 80% of the chord before coming to around 0 at the trailing edge. Over the same region, the lower surface, Fully stall - Bottom, stays near 0 and goes into negative pressure at the same point along the chord where the upper surface peaks at around 0.7. This rapid loss of suction and collapse of the pressure difference is an indicator of separation. At the leading edge, the difference between the upper and lower surfaces is large but by the mid-aft chord, the difference has fallen to less than 1. Instead of showing recovery, the upper surface C_p rises to around 0, leaving little pressure difference across the chord. This shows that the flow has separated over much of the upper surface, explaining the sharp reduction in lift, in the stalled condition. Similar trends are also observed at 15m/s in the wind tunnel, confirming that this separation behavior is not unique to 30 m/s but is a consistent feature of stall.

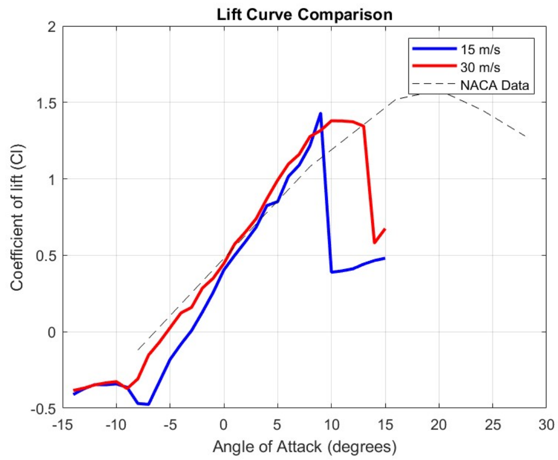

Fig. 5

For Figure 5, the coefficient of lift was plotted against the angle of attack.This graph was not produced simply plotting collected data. The points for this graph were produced by computing an integration of the pressure distribution which demonstrated the axial forces, which give a numerical base for the lift calculations that followed. It was found through the two data sets that not all angles of attack produce high coefficients of lift. For example, it was found in both data sets that angles of attack from -10 degrees to around -7 degrees produced very little or negative coefficients of lift. Conversely, for both the 15 m/s and the 30 m/s data, it was also observed that there were other angles of attack that created high coefficients of lift. For example, in the 15 m/s data set, the maximum coefficient of lift was around 1.4 with an angle of attack around 8 degrees. Additionally, in the 30 m/s data set, the data shows a more gradual climb up to a maximum lift coefficient of around 1.3 with the angle of attack of 10 degrees. While analyzing the graph, consideration was given to lift curve slope. In this figure, it was noticed that both data sets do not act completely linearly. Due to this fact, determining a precise lift curve slope is difficult, however, there are some ranges of angles that do function linearly. For example, in the 15 m/s curve, after the maximum lift coefficient, a drop off from after 8 degrees to 10 degrees acts linearly. In the 30 m/s curve, a linear drop off is also seen but after a leveling off. At 12 degrees to 13 degrees there is a shallower linear slope of around -0.2 and at 13 degrees to 14 degrees, a steeper slope around -2.5 is displayed. While there are a few more linearly acting ranges of the curves, those mentioned above contain the major ranges that help to inform about the differences across the tests.

III. Conclusions

In the examining of the results of the data collected and computed, the graph of Coefficient of Lift vs Angel of Attack shows that our results from 0° to 5° match the NACA results. From -15° to 7° the NACA results have a much shallower lift curve slope, with its slope value being around .75 while the test data for 15 m/s and 30 m/s sets had lift curve slopes greater than 1. Around the respective stall angles for the 15 m/s, 30 m/s and NACA report there was also a greater observable difference. The collected data stalled at 10 ° for 15 m / s and 15 ° for 30 m / s, while the NACA Report data appear to stall around 20 °. This is a full 10 degree difference from the 15 m/s collection. This difference in values likely stems from inconsistent Reynolds numbers between both experiments. In the NACA report, the Reynolds number (Re) was about 3×10^6, a greater value than could be created within the wind tunnel used for the data collection in these tests conducted in class. The greater Reynolds number in the NACA report meant that the airfoil could reach a higher Coefficient of Lift before stalling, which is reflected in Figure 5. These results help to illustrate the relationship between angle of attack and coefficient of lift, pressure distribution, and velocity. Using an angle of attack between 2° and 8° which gives a Coefficient of Lift without chance of stall, and allows us to estimate what the conditions should be aimed for when designing the gliders. Understanding the Coefficient of Pressure and how its distributed about the airfoil also allows visualization of how pressure impacts lift and overall performance of the airfoil in typical angles of attack around 6° for flight. Finally, understanding the velocity of air as it moves over the airfoil allows for an understanding and demonstration of stream tubes, and a visualization of how air moves and changes speed as it interacts with the airfoil. All of these understandings and relationships give insight into fundamental principles that govern flight and will allow for more data supported decision making when it comes time to choose what kind of airfoil will be emulated in the glider design.

Acknowledgments

Professor Hoke and the Teaching Assistant/ Facilitator Team

References

[1] AIAA. Journal scopes and content.

[2] J D Anderson and M L Bowden. Introduction to Flight, chapter 2 - 6. Mc Graw Hill, New York, 9 edition, 2022.

[3] R M Pinkerton and H Greenberg. Aerodynamic characteristics of a large number of airfoils tested in the variable-density wind tunnel, 1938. 15 of 23